Publication Year	2024
Acceptance in OA	2024-09-24T09:33:12Z
Title	Detailed cool star flare morphology with CHEOPS and TESS
Authors	BRUNO, Giovanni, PAGANO, Isabella, SCANDARIATO, GAETANO, Florén, H. G., Brandeker, A., Olofsson, G., Maxted, P. F.L., Fortier, A., Sousa, S. G., Sulis, S., Van Grootel, V., Garai, Z., Boldog, A., Kriskovics, L., Szabó, Gy M., Gandolfi, D., Alibert, Y., Alonso, R., Bárczy, T., Barrado Navascues, D., Barros, S. C.C., Baumjohann, W., Beck, M., Beck, T., Benz, W., Billot, N., BORSATO, LUCA, Broeg, C., Collier Cameron, A., Csizmadia, Sz, Cubillos, P. E., Davies, M. B., Deleuil, M., Deline, A., Delrez, L., Demangeon, O. D.S., Demory, B. O., Ehrenreich, D., Erikson, A., FARINATO, JACOPO, Fossati, L., Fridlund, M., Gillon, M., Güdel, M., Günther, M. N., Heitzmann, A., Helling, Ch, Hoyer, S., Isaak, K. G., Kiss, L. L., Lam, K. W.F., Laskar, J., Lecavelier des Etangs, A., Lendl, M., MAGRIN, DEMETRIO, Mordasini, C., NASCIMBENI, VALERIO, Ottensamer, R., Pallé, E., Peter, G., Piotto, G., Pollacco, D., Queloz, D., RAGAZZONI, Roberto, Rando, N., Ratti, F., Rauer, H., Ribas, I., Santos, N. C., Sarajlic, M., Ségransan, D., Simon, A. E., SINGH, VIKASH, Smith, A. M.S., Stalport, M., Thomas, N., Udry, S., Ulmer, B., Venturini, J., Villaver, E., Walton, N. A., Wilson, T. G.
Publisher's version (DOI)	10.1051/0004-6361/202348951
Handle	http://hdl.handle.net/20.500.12386/35317
Journal	ASTRONOMY & ASTROPHYSICS
Volume	686

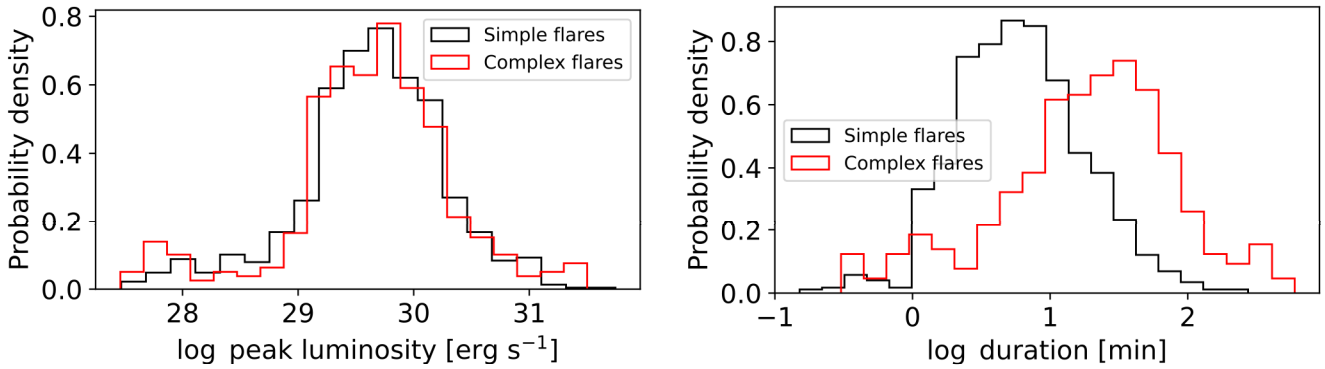

Fig. 10. Distribution of flare luminosity (left) and duration (right) for single-peaked (black) and individual components of multi-peaked (red) flares.

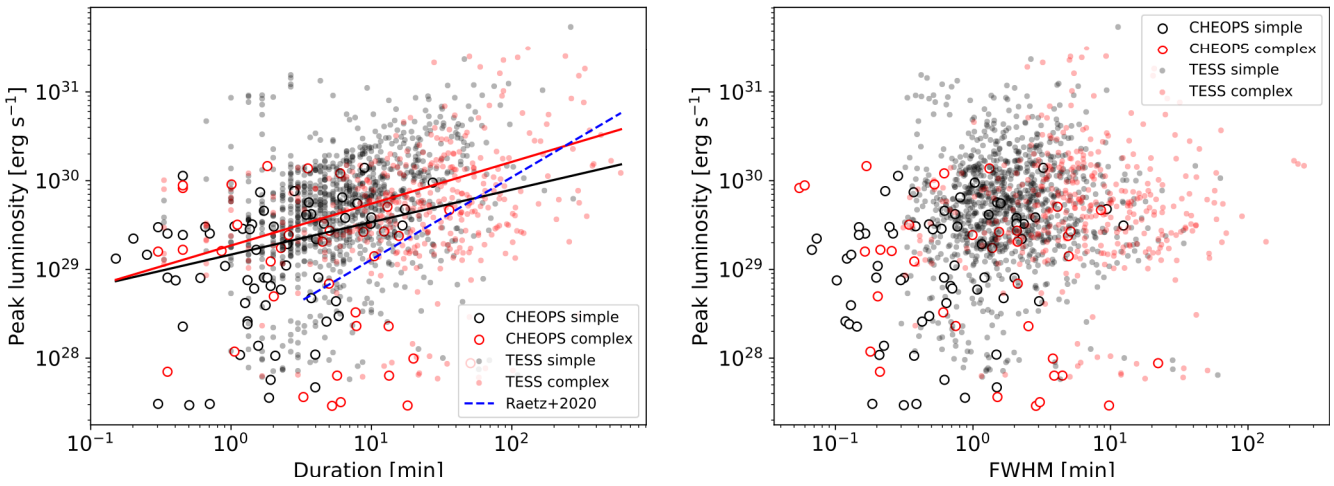

Fig. 11. Flare parameter trends. Left: relationship between flare peak luminosity and duration. Simple and multi-peak flares are separated, as well as the instrument they were detected with. The trend found by Raetz et al. (2020) is shown for the sake of comparison. Right: relationship between flare luminosity and FWHM.

two effects were found to compensate in K2 when integrated energy levels are computed (Raetz et al. 2020).

Even if the flare *L-d* trend is instrument-dependent, it can be informative if comparisons are made among subsets of events observed in the same setting. We confirm the trend holds when including higher-cadence data: in particular, we found a Pearson correlation coefficient of 0.46 (p-value for non-correlation $\sim 10^{-56}$) and 0.28 ($p \sim 10^{-8}$) for simple and complex flare components, respectively. We estimated the coefficients of an *L-d* linear relationship by bootstrapping 1000 times every validated flare's amplitude and FWHM based on their mean value and uncertainty; L and d were re-calculated at each iteration from the corresponding profile. The fits revealed two different slopes for the simple and complex flare trends, which might be explained by their different duration distributions:

$$\log L_{\rm simple} = (0.36 \pm 0.01) \log d_{\rm simple} + (29.17 \pm 0.02) \quad (6)$$

and

$$\log L_{\rm complex} = (0.48 \pm 0.01) \log d_{\rm complex} + (29.27 \pm 0.01), \quad (7)$$

where luminosity and duration are measured in erg s^{-1} and minutes, respectively. The measurements and fits are shown in the left panel of Fig. 11. Some of the validated flares had very small uncertainty on one or both amplitude and FWHM: as this was probably a numerical effect due to the minimisation algorithm, we reduced the weight of these events by assigning a relative uncertainty of 10% to all parameters with relative uncertainty $<10^{-2}$ on any of these parameters (5% of the flares).

The fitted coefficients for the *L-d* relationship are significantly lower than the ones found by Raetz et al. (2020), who reported a linear coefficient of 0.93 ± 0.04 on the K2 short cadence (≃1 min) data of M stars with a wide variety of activity levels: this can be explained by the differences among Kepler, CHEOPS and TESS. Interestingly, Brasseur et al. (2019) did not find a significant correlation between flare luminosity and duration, using a sample of 1904 flares observed at 10 s cadence with GALEX near-UV.

Constraining the *L-d* relationship might help refine the models used to compute the energy flares can deposit onto exoplanet atmospheres, and particularly to scale the prototypical flare profiles that are used (e.g. Nicholls et al. 2023). In this regard, the flare FWHM is a proxy for the time during which the emission rises and decays more rapidly. For example, Venot et al. (2016) modelled the flare-induced chemical perturbations that might occur in simulated planetary atmospheres, by exposing them to observed AD Leo flare spectra during their impulsive rise, impulsive decay and gradual decay phases, and found that the effect on an atmosphere is more significant during the impulsive phases.

We therefore turned to look for trends between flare peak luminosity and FWHM, for which neither simple nor complex flares showed any significant correlation. The relationship

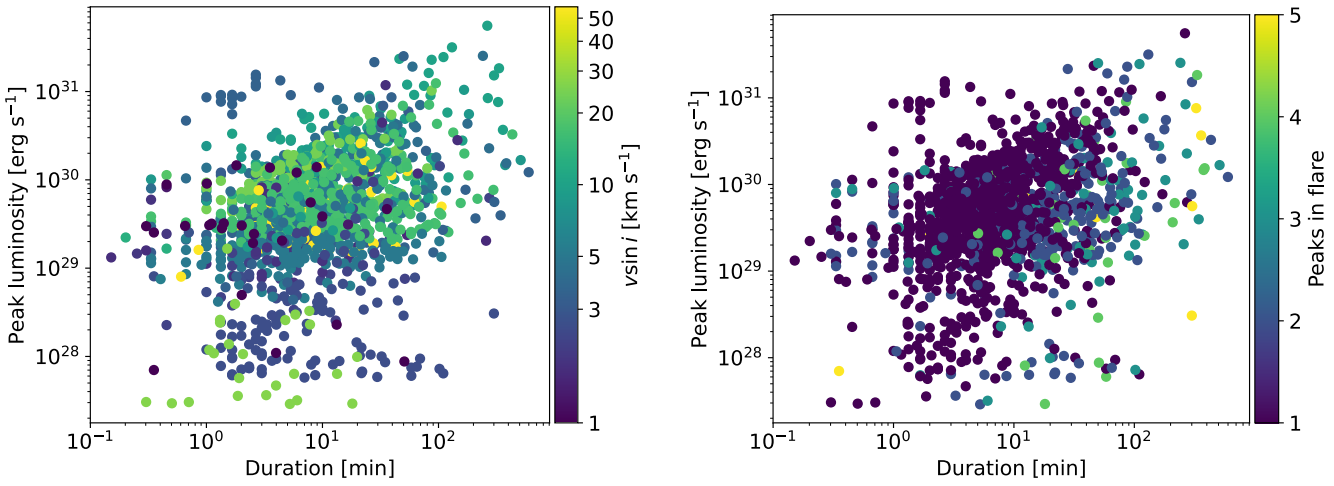

Fig. 12. Flare parameter trends. Left: relationship between flare luminosity and duration, where the stellar $v \sin i$ is represented with the marker colour. Right: same relationship, where the flare complexity is represented with the marker colour. We remind that each point represents a single outburst even in a multi-peak flare, so that the colour refers to the complexity of the event each data point belongs to.

between the two parameters is shown in the right panel of Fig. 11, and the associated Pearson correlation coefficients have p-values of 0.62 and 0.73 for single and multi-peak flare components, respectively.

Finally, we remark that the flares with the largest duration and peak luminosity are also associated with higher stellar rotation levels and complexity. Figure 12 shows the relationship between these parameters, by colouring the flare L-d pairs according to the stellar $v \sin i$ on the left, and the number of flare peaks on the right. Despite the fact that low $v \sin i$ values might be both due to a truly low rotation velocity or to highly inclined stellar rotation axes with respect to the plane of the sky, we qualitatively recovered the same finding as Raetz et al. (2020), who used actual stellar rotation periods as a proxy for stellar activity.

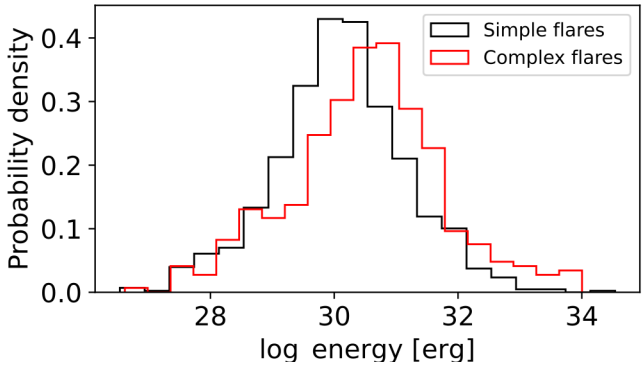

Fig. 13. Distribution of computed flare energies. Single-peaked and individual components of multi-peaked flares are coloured in black and red, respectively.

6.4. Flare energy

Flare energies were calculated following Davenport (2016), that is, by multiplying the quiescent flare luminosities by the integral under the flares (which is measured in time units). The median energy value is similar between simple and complex flare components: 1.3×10^{30} and 3.4×10^{30} erg, respectively. However, Fig. 13 shows a difference in the high-energy part of the respective distributions: the hypothesis that the two of them belong to the same one is rejected by a KS test with a p-value of $\sim 10^{-11}$. This is due to the fact that the complex flare component distribution has a larger number of events in the 10^{31}–10^{34} erg range compared to simple events.

Based on a simple model of the energy E released during a magnetic reconnection event, Maehara et al. (2015) suggested that on solar type stars flare duration d relates to the event energy as $d \propto E^{1/3}$. This relationship was in agreement with their findings on superflares observed on solar-like stars with Kepler short-cadence data, as well as with Namekata et al. (2017)'s results on solar-like stars white-light flares. Different trends were found by Brasseur et al. (2019)'s measurements on GALEX near-UV, and well as by Pietras et al. (2022) and Yang et al. (2023) on a wider range of spectral types with TESS 2 min data. Deducing from these results a difference in the underlying flare generation process in different types of stars is far from trivial, as it requires budgeting the respective instrumental characteristics. For our dataset, shown in Fig. 14, we inspected the flare duration-energy dependence by separating simple and complex flare components, and carrying out a bootstrap fit as for flare luminosity and duration. This yielded

$$\log d = (0.296 \pm 0.004) \log E - (8.1 \pm 0.1) \quad (8)$$

and

$$\log d = (0.37 \pm 0.01) \log E - (10.1 \pm 0.2) \quad (9)$$

for simple and complex flare components, respectively; here, d is measured in min and E in erg. The flares we detected lie in a lower-energy, wider duration region of the parameter space than the one explored by the aforementioned authors (see e.g. Fig. 21 in Brasseur et al. 2019), and are broadly in agreement with Maehara et al. (2015)'s model.

As flare impulse $\mathcal{I}$ informs on the most impactful phases of a flare in the surrounding environment, we explored its relationship to flare energy. Even if the integrated energy is comparable at different cadence (Raetz et al. 2020), we statistically observed that the measured impulse tends to increase with time resolution. This is illustrated in Fig. 15, where we show the flare impulse and energy for our data set at native (3 and 20 s for CHEOPS and TESS, respectively) and binned to 1-min cadence; when analysing the binned data, we rescaled the retrieved parameters

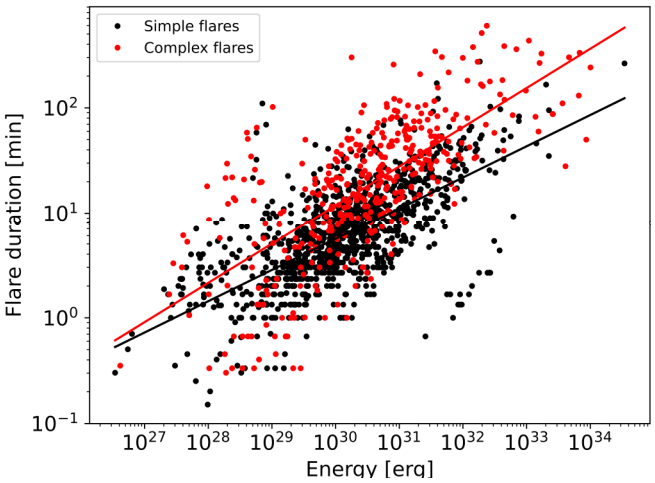

Fig. 14. Flare duration vs. energy, divided in simple (black) and complex (red) outburst components.

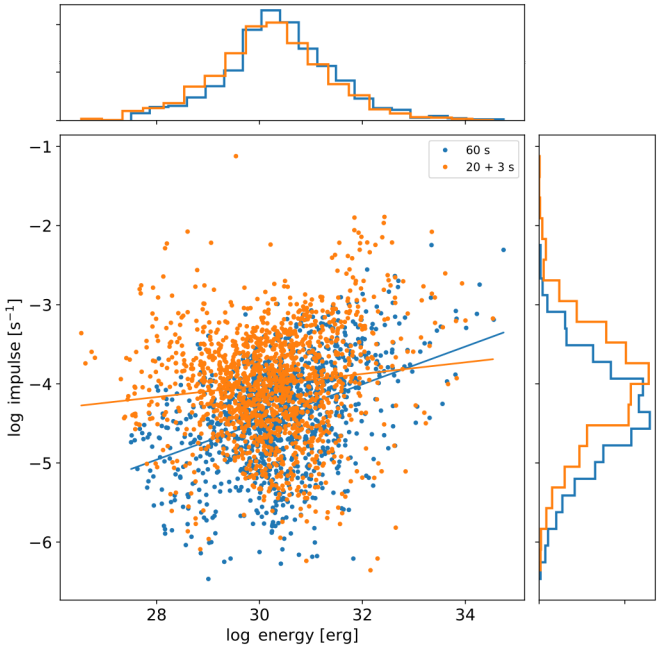

Fig. 15. Relationship between flare impulse and energy at native (orange) and binned to 1-min (blue) cadence. The upper and right panels show the energy and impulse marginalised distributions, respectively.

on the basis of injection tests using light curves rebinned at the same cadence.

More in detail, the impulse distribution at native cadence is significantly shifted to higher values with respect to the binned-data distribution: the two of them are distinguished with p-value $\sim 10^{-33}$ by a KS test. We also recovered two different trends for the data at native and binned cadence, that is,

$$\log \mathcal{I} = (0.073 \pm 0.004) \log E - (6.2 \pm 0.1) \tag{10}$$

and

$$\log \mathcal{I} = 0.238^{+0.005}_{-0.006} \log E - (11.6 \pm 0.2) \tag{11}$$

for native and binned cadence, respectively, and where impulse is measured in s^{-1}. This suggests that the high-time resolution monitoring of stellar hosts might be a relevant factor to correctly estimate the impact of high-rate, low-energy flares onto the evolution of exoplanet atmospheres.

6.5. Parameter distributions

The flare energy distribution is generally assumed to follow a power law, that is,

$$N(x)\,\mathrm{d}x \propto x^{-\alpha}\,\mathrm{d}x, \tag{12}$$

with $\alpha > 0$, in the so-called 'inertial range' $x_1 \leq x \leq x_2$. In this case, x is flare energy. One of the hypotheses to explain this behaviour is that stellar flares are Self-Organised Critical (SOC) systems (Bak et al. 1988; Lu & Hamilton 1991), which are known for their fundamental properties such as spatial extension, duration and delivered energy to be at least partly scale-invariant. Standard SOC system parameters such as peak flux, duration, and energy are distributed according to power laws, but slight deviations might provide indications about the mechanisms that power them (Kunjaya et al. 2011). For example, extreme or 'Dragon-King' events might depart from this relationship (Sornette 2009; Sornette & Ouillon 2012), and a statistical exploration of their distributions might add constraints to investigations based on purely physical principles (Karoff et al. 2016). The detection of irregularities with respect to theoretical power laws and other expected SOC properties is also made possible by the ever-increasing precision in observations (e.g. Sheikh et al. 2016), and might provide insights on mutually triggered, sympathetic flares (Aschwanden 2019). In particular, Dragon-King events appeared to be rare in a sample of hard X ray solar and Kepler stellar flares (Aschwanden 2019). However, complex flare events are not often split into their individual components, which might carry a certain contamination from memory processes (Lei et al. 2020): with the algorithm we developed, we explored whether the contribution from complex outbursts can be distinguished from the one of single-peaked events. While we did not explore the likelihood of complex outbursts as being due to actual sympathetic flares or to independent simultaneous events (e.g. Wheatland 2006; Wheatland & Craig 2006), we consider at least a part of the complex outbursts we observed to be likely sympathetic.

Several factors need to be taken into account when fitting power laws, and one of the most crucial is to estimate the likelihood that other distributions might better represent the data. Following Verbeeck et al. (2019), we chose a log-normal distribution as a plausible alternative, as it might indicate the need for a revision of the basic flare triggering mechanisms. This might be necessary, for example, if not all magnetic energy were released during an outburst (Kunjaya et al. 2011), if its originating magnetic elements went through a fragmentation process (Bogdan et al. 1988), or also if flares were a result of MHD turbulence, as was suggested from the study of flare waiting times (Boffetta et al. 1999; Greco et al. 2009; Norman et al. 2001; Watkins et al. 2016; Lei et al. 2020). Comparing the description of flare parameter distributions can provide additional details to this decades-long-debate.

In the analysis here presented, we neglected the differences between the stars in our sample and considered them to be representative of a 'prototypical' late-K/M star, in order to increase the statistics on the parameter distributions. We fitted the slope α for the flare energy, peak luminosity, and duration distributions following Clauset et al. (2009) and Klaus et al. (2011)'s prescriptions. This method is at least as statistically stable as a fit to a log-log histogram and can provide the likelihood ratio between a power law and another model description of the data. Moreover, it allows a formal determination of x_1 (see Eq. (12)) through minimisation of the KS distance between the data and the model.

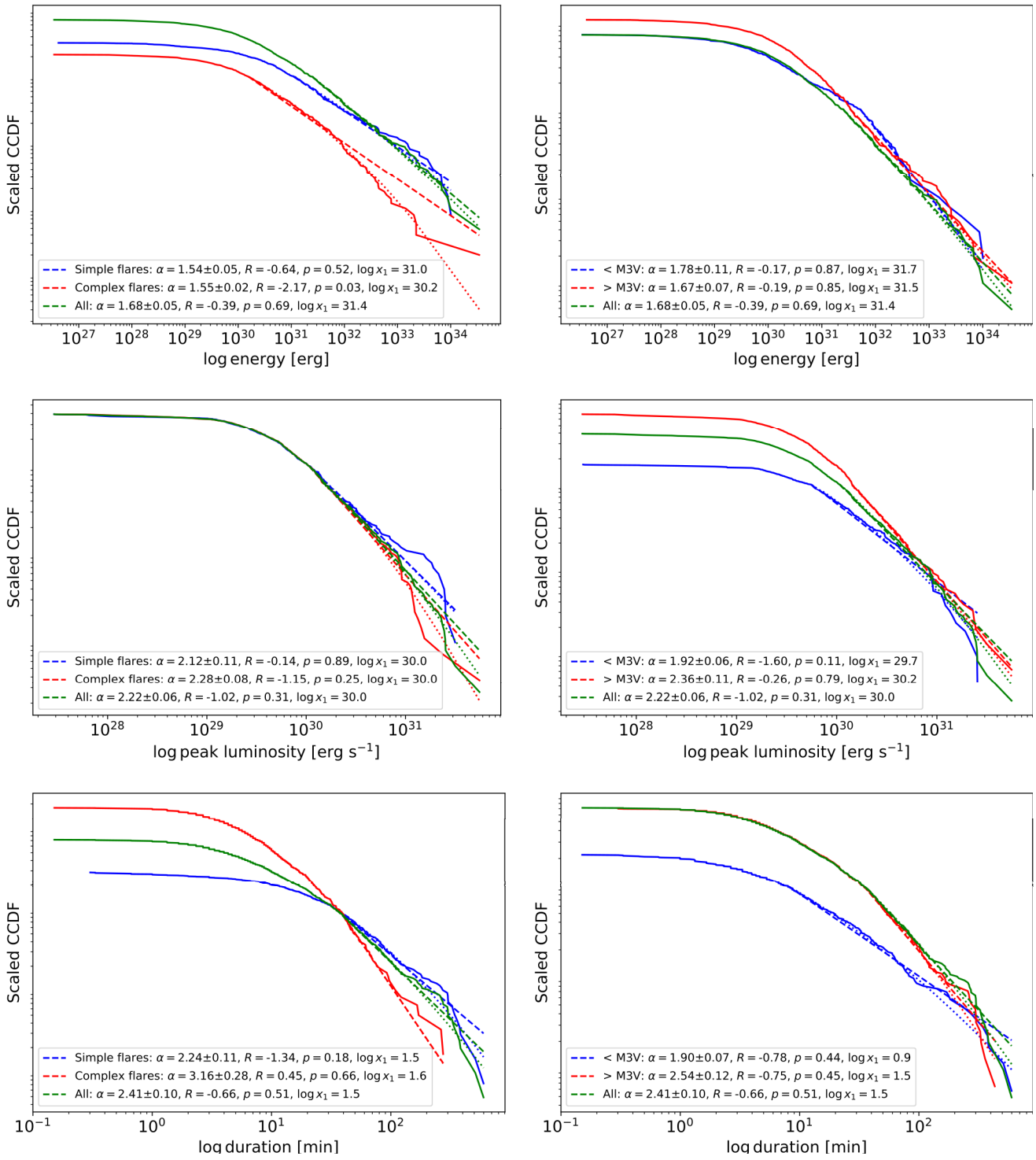

Fig. 16. Complementary cumulative distribution functions (CCDFs) for flare parameters. Left column: scaled complementary cumulative distribution functions (CCDF) for flare energy (top), peak luminosity (centre) and duration (bottom), separated between simple flares (blue), complex flare components (red), and the full sample (green). Observed distributions, power-law fits, and log-normal distribution fits are represented with lines, dashed lines, and dotted lines, respectively. Right column: same as the left column, but where the flare sample is divided in events occurring on stars earlier (blue) or later (red) than M3V. In each panel, the legend indicates the fitted power-law coefficient α, the normalised likelihood ratio R between the power-law and log-normal fits, its associated p-value, and the lower bound of the inertial range used for the fit, x_1.

This is another key aspect in the estimation of power law parameters, which is often left to subjective evaluation. Adopting similar statistical tools, Verbeeck et al. (2019) found that a log-normal distribution is a preferred description for a sample of about 17 000 solar X-ray flares collected between 2010 and 2018.

For our analysis, we used the POWERLAW package (Alstott et al. 2014), where the above described statistical framework is implemented. The top-left panel of Fig. 16 shows the complementary cumulative distribution function (CCDF) of the observed flares as a function of their bolometric energy E for

Table 2. Fitted power-law coefficients α, normalised likelihood ratio R, corresponding p-value, and lower bound for the inertial range x_1 for the cumulative distribution of each flare parameter and subset.

	α	R	p-value	x_1 [log erg]
Simple flares				
Energy	1.54 ± 0.05	-0.64	0.52	31.0
Peak luminosity	2.11 ± 0.11	-0.14	0.89	30.0
Duration	2.24 ± 0.11	-1.34	0.18	1.5
Complex flare components				
Energy	1.55 ± 0.02	-2.17	0.03	30.2
Peak luminosity	2.28 ± 0.08	-1.15	0.25	30.0
Duration	3.16 ± 0.28	-0.01	1.00	1.6
Partially convective stars				
Energy	1.78 ± 0.11	-0.17	0.87	31.7
Peak luminosity	1.92 ± 0.06	-1.60	0.11	29.7
Duration	1.90 ± 0.07	-1.18	0.24	0.9
Fully convective stars				
Energy	1.67 ± 0.07	-0.19	0.85	31.5
Peak luminosity	2.36 ± 0.11	-0.26	0.79	30.2
Duration	2.54 ± 0.12	-0.84	0.40	1.5
All stars				
Energy	1.68 ± 0.05	-0.39	0.69	31.4
Peak luminosity	2.22 ± 0.06	-1.02	0.31	30.0
Duration	2.41 ± 0.10	-0.91	0.35	1.5

flares with only one or multiple resolved components, respectively. In this and the following panels of the same Figure, the CCDF has been scaled to its value at x_1. The fitted value for α, the normalised likelihood ratio R of the power law against log-normal model, the corresponding p-value against the null hypothesis of the descriptions being equivalent and the lower bound of the inertial range used for the fit x_1 are reported in Table 2 ($R > 0$ indicates a preference for the power law description, and $R < 0$ the alternative case). The α values for the two distributions are in agreement and are both compatible with most results in the literature, and particularly with the 1.50–1.75 range of flare avalanche models (e.g. Litvinenko 1996). However, we notice the energy distribution of complex events is poorly fitted by a power law, and that a log-normal is a better description with a p-value of 0.03. For the single-peak and the combined distribution of single and combined events, the preference for a log-normal is only marginal, so that we can compare them to the predictions of SOC models: in particular, a standard SOC model with $\alpha = 1.44$ (Aschwanden 2022a) is in 2σ agreement with our results for the simple flare distribution, contrarily to Aschwanden (2022b)'s three-dimensional fractal energy model. This latter is characterised by $\alpha = 1.80$, which is at 5σ distance from the result for simple events, but within 2.5σ from the combined distribution fit.

We repeated the same test for flare peak amplitude and duration, and report our results in the middle and lower panels in the left column of Fig. 16. Here, the α slopes predicted by the standard SOC model for peak flux and avalanche duration are $\simeq$1.67 and 2 (Aschwanden 2022a), and are 9 and 4σ away from our results for the combined distributions, respectively. Overall, we found a 2σ agreement for the peak luminosity distribution of simple and complex flare components, and a 3.3σ distance for the respective duration distribution parameters.

The most recent evaluations of α in the flare energy distribution used large samples of 2 min cadence data from the TESS mission, and reported no significant variation of the power law index within earlier and later M stars (Feinstein et al. 2022). The current debate is open, as a tentative α dependence on spectral type was found in other studies (e.g. Yang et al. 2023). This motivated us to inspect the parameter distributions for partially convective (spectral type earlier than M3V) and fully convective (later than M3V) stars, without distinguishing simple and complex flare components. In the right column of Fig. 16, we plot the corresponding flare energy, peak luminosity and duration scaled CCDFs. The α indices of the energy distributions are in $\sim 1\sigma$ agreement, while the luminosity and duration distributions are at 4–5σ distance. The energy distributions, moreover, are compatible with the 1.50–1.75 range in both cases, as well as at 2σ agreement with the three-dimensional fractal energy model. In this analysis, selection effects cannot be excluded, as the flare S/N, which peaks at short wavelengths, is expected to increase for redder and cooler stars. For these latter, the detection of low-energy events might be easier, given the same photometric noise level.

In terms of the comparison between power-law and log-normal descriptions of the parameter distributions, we found variations depending on the parameter and subset, but in all cases only marginal. To inspect whether a larger sample could increase the statistical significance of one model description compared to the other, for each outlined case we used POWERLAW to simulate data sets corresponding to the fitted power law parameters, each with 10^4 samples. For each of these data sets, we fitted another power law and log-normal distribution, and compared the resulting likelihood ratio. We found that the duration distributions could be better constrained with a larger sample, a fact that could be addressed by further dedicated analyses.

6.6. Pre-flare dips

To inspect for pre-flare dip candidates, we filtered our dip fits and selected only those with (1) ΔAIC $>$ 6 with respect to the model without dip, (2) a $S/N > 2.5$ for the dip amplitude with respect to the correlated noise level in a time window as wide as the fitted dip, (3) an overall flare reduced $\chi^2 < 10$, and (4) a dip duration of at least three data points (measured as the sum of the dip width on both sides). In Fig. 17, we display the dip candidates that passed these criteria, and colour the points according to the duration of the associated flare (or the total duration of the outburst in case of a complex flare). We report this information because, by visual inspection, we noticed that in most cases the dip is associated with long-duration flares, where it is likely that the light curve smoothing process has artificially reduced the flux before the rise phase of the flare, creating a false dip effect.

After a visual inspection, we only retained one event as valid dip candidate, which is illustrated in Fig. 18. It was observed with CHEOPS on V1054 Oph: interestingly, a multi-band pre-flare dip was reported by Ventura et al. (1995) on the same star. The relative amplitude of the candidate, which occurred $\simeq$2.7 min before the beginning of the corresponding flare, is $(0.17 \pm 0.02)\%$, and its width (47 ± 13) s. Its following flare was also very little energetic, with $E \simeq 6.6 \times 10^{28}$ erg: this is one of the smallest energies we measured. Comparatively, the one found by Ventura et al. (1995) right before a flare event had a relative amplitude of $(6 \pm 3)\%$ in the V band, and an exceptional duration of $\simeq$36 min. Its following flare could not be observed in the V band, but presented $E = 1.66 \times 10^{32}$ erg in the B band. Its lack

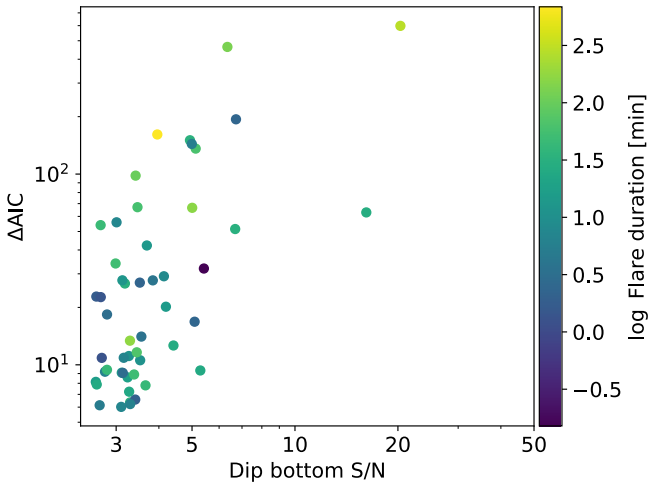

Fig. 17. Pre-flare dip AIC between a model including a pre-flare dip and a model without it as a function of the candidate dip S/N. Only dips with the criteria outlined in Sect. 6.6 are shown.

of visibility in the *V* band might make it comparable to the very small-energy flare we detected.

All in all, no information that could have helped us validate our candidate was available in other wavelengths. Therefore, we consider our detection only tentative, and refrained from a more detailed analysis.

6.7. Quasi-periodic pulsations

QPPs can be empirically distinguished from multi-peak flares by the quasi-periodicity of the flux rises and decays. We visually searched for QPP candidates in our validated complex flares: as our algorithm does not model QPPs, it is likely that some of them are misinterpreted as multi-peak flares. After rejecting those with the most irregular sequences of sharp peaks and smooth 'bumps', we isolated one and 14 QPP candidates in the CHEOPS and TESS light curves, respectively: this is about 1% of the full sample, close to recent reports (Balona & Abedigamba 2016; Pugh et al. 2016). One of our candidate QPPs is shown in Fig. 19: in the left panel, we show the highest-likelihood multi-peak flare model, which we used to extract the mean periodicity of the oscillation as the average distance between consecutive flare peaks. On the right panel, we show a model with a single, smooth-peak flare shape fitted on the complex flare profile: from the half-difference between the largest and smallest flux values we extracted the oscillation amplitude. Following Howard & MacGregor (2022), we examined the ratio between this quantity and the amplitude of the single-peak flare used to derive the flux residuals. The other candidates, on which we applied the same method, are reported in Appendix B. The 'waiting times' we determined span the 4–50 min range, in agreement with previous results (e.g. Pugh et al. 2016; Vida et al. 2019; Ramsay et al. 2021; Million et al. 2021; Howard & MacGregor 2022).

In Fig. 20, we plot the QPP parameters we derived as in Howard & MacGregor (2022), and recovered similar tentative correlations: in particular, a negative trend between flare energy (i.e. the single-smoothed flare fitted to the complex profile) and oscillation amplitude, and a positive trend between flare energy with the QPP duration.

To be conservative, the flare sample just presented was not included when deriving flare parameters in the previous parts of this study (even if we verified that it does not significantly affect any result). Additionally, we assessed the possible contamination of undetected QPPs in the fits of all the other flare profiles. To do this, we first examined the periodicities with False Alarm Probability (FAP) < 1% that emerged from the Lomb-Scargle periodograms (LSP) of the flare fit residuals. The calculation was carried out using Baluev (2008)'s method, implemented in the `astropy` tools we used: 18% of the flare residuals present significant peaks, and their histogram is shown in Fig. 21. The median peak of the distribution corresponds to ≃67 min, which is larger than the duration of most complex flare components (right panel of Fig. 10), time delay between consecutive flares (Fig. 9), and reported values in the literature for QPP periods, which span the ∼2–72 min range (e.g. Pugh et al. 2016; Vida et al. 2019; Ramsay et al. 2021; Million et al. 2021; Howard & MacGregor 2022); from this calculation, we excluded a candidate found on AD Leo, highlighted in Appendix B, because of its corresponding poor fit. This suggests that the correlated signal present in some residual light curves is not related to QPPs, but to uncorrected systematics or poor fits; we recall that we consider unlikely for stellar granulation to be detectable in our light curves, given their S/N and the granulation expected signal.

6.8. Undetected flares and light curve scatter

Stelzer et al. (2016) reported a correlation between photometric scatter in the detrended light curves and stellar rotation period, and argued that this might be a signature of undetected starspots or flares. As shown in Fig. 22, we observed a similar relationship for the targets for which we have a $v \sin i$ measurement. The Pearson correlation coefficient between the two quantities excludes the no-correlation hypothesis with a p-value of $\sim 10^{-19}$ and 10^{-5} for TESS and CHEOPS data, respectively. The positive correlation in TESS light curves is mainly driven by the points with RMS > 5000 ppm, which correspond to GJ 65, GJ 3304, G 214-14 and AD Leo, which we inspected to exclude any anomaly.

However, contrarily to Stelzer et al. (2016), we also noticed a very strong correlation between flattened light curve RMS and stellar magnitude, as shown in Fig. 23. This makes the impact of stellar activity features in the photometric scatter unlikely in our case.

We remark, moreover, that a pooled variance analysis (Dobson et al. 1990; Donahue & Baliunas 1992; Donahue 1993; Lanza et al. 2003) of the flattened CHEOPS light curves does not seem to approach any 'basal level' in the light curves scatter. This might be related, for example, to an approaching 'flare background', as suggested by Stelzer et al. (2016), and would correspond to a flattening in the pooled variance at the lowest cadences. The pooled variance of our CHEOPS observations is shown in Fig. 24.

7. Discussion and conclusions

The use of high-cadence, high precision photometry from CHEOPS and TESS allowed us to probe unexplored regions of the white-light flare parameter space in late-K and M stars. In this study, moreover, we adopted the same analytical model for the profile of single-peak and multiple-peak outbursts, and searched for differences in the distributions of the respective flare luminosity, duration, and energy. Using this, we also investigated whether power laws are the most likely description for simple and complex flare parameter distributions, as most studies generally assumed, but which has recently been challenged in studies of solar flares. Finally, we inspected for the presence of

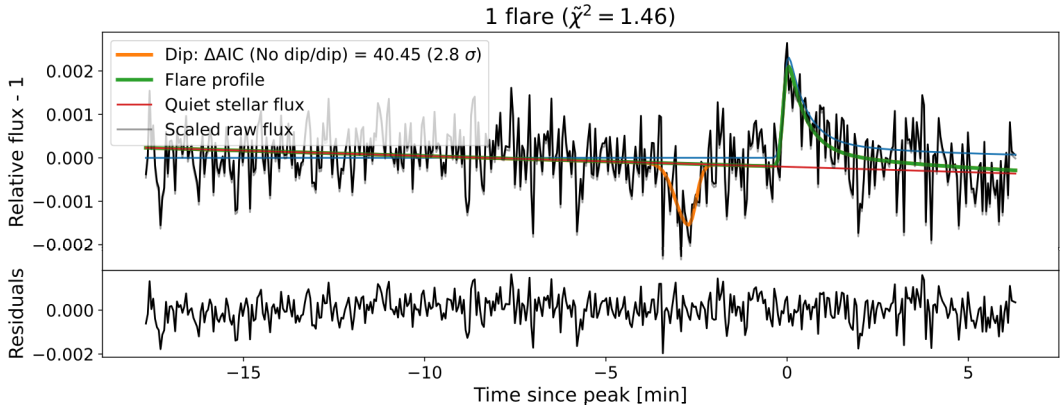

Fig. 18. Pre-flare dip tentative detection on V1054 Oph.

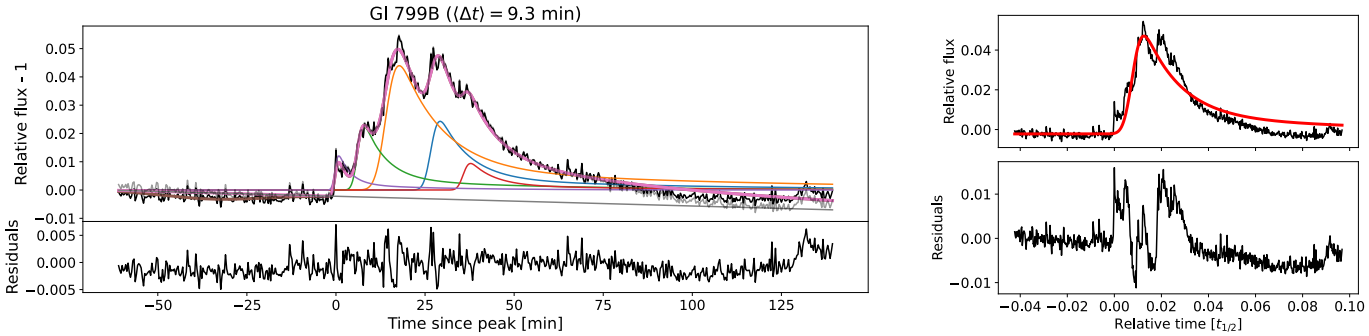

Fig. 19. QPP candidate on Gl 799 B. Left: the mean time between consecutive peaks is reported in the title. This QPP candidate is probably the same one reported by Howard & MacGregor (2022; their Fig. 7, left panel), for which we recover a similar period to their ≃7.5 min. The individual flare components that were identified by our algorithm are drawn with different colours, and the total model is represented with a thick line. Right: on the top sub-panel, fit to the flare profile with a single-peak model. On the lower sub-panel, the residuals used to estimate the oscillation amplitude.

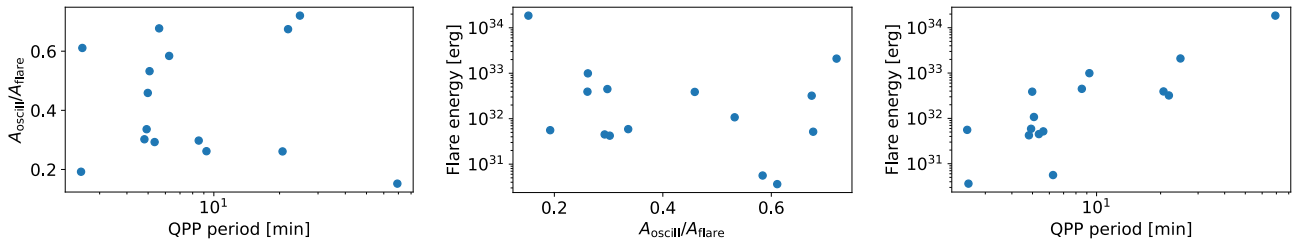

Fig. 20. Relationships between estimated QPP parameters.

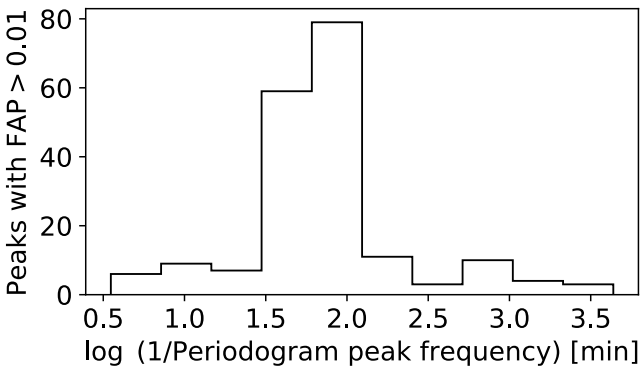

Fig. 21. Histogram of the flare residuals periodicity corresponding to LSP peeks with FAP< 1%.

pre-flare dips and MHD-driven QPPs, and found no indication of an undetected flare background below the data noise level.

We confirmed the results by Hawley et al. (2014), who found that complex flares can reach longer durations than simple events, even after the individual flare components are resolved. We did not retrieve significant differences between flare parameter correlations for events lasting more than a few minutes (already thoroughly investigated with *Kepler*/K2 and 2-min TESS data in previous works) and shorter ones. However, our analysis suggests higher flare impulses can be reached on cool stars, compared to previous findings. This indicates that high-cadence photometric monitoring of planet hosts might be crucial to correctly estimate the high-energy, time-limited flux exoplanet atmospheres might be exposed to. At lower cadence, the high-impulse stellar irradiation might be missed, and the only flare energy distribution might provide incomplete information to compute trustworthy models for planetary atmospheres. The amount of deposited energy is needed to compute, for example, variations in ozone abundance and rates of water photolysis (e.g. Segura et al. 2010; Loyd et al. 2018). This result

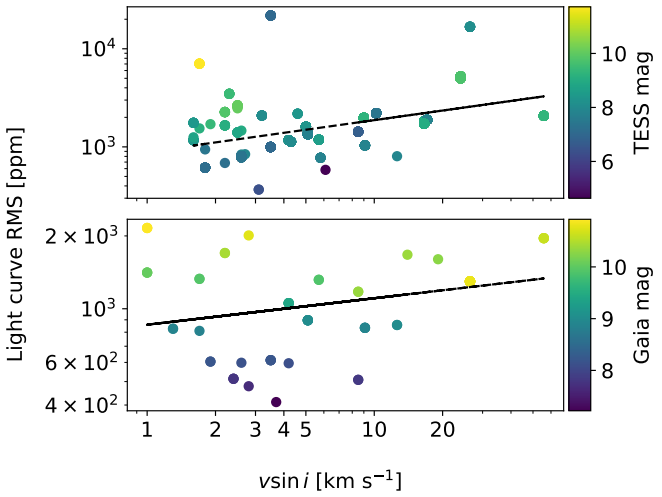

Fig. 22. Correlation between flattened light curve scatter (y-axis) and stellar $v \sin i$ (x-axis) for the stars for which this quantity was available. TESS and CHEOPS are represented in the top and bottom panel, respectively. A log-log fit is shown with a dashed line.

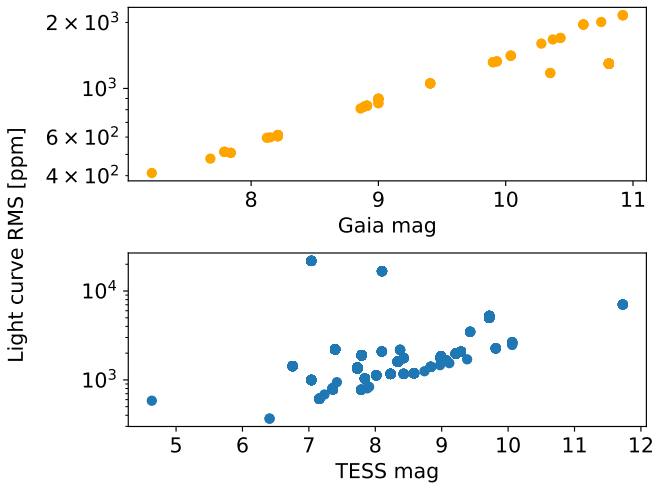

Fig. 23. Correlation between flattened light curve scatter (y-axis) and stellar magnitude. CHEOPS observations with *Gaia* magnitudes and TESS light curves with TESS magnitudes are represented in the top and bottom panel, respectively.

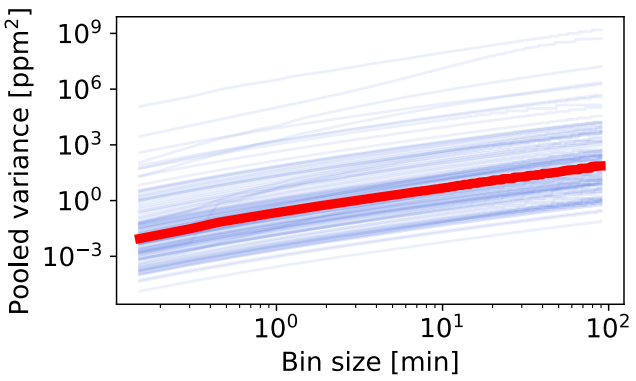

Fig. 24. Pooled variance of the detrended CHEOPS light curves as a function of bin size, shown with blue lines. The median pooled variance curve is shown with a thick red line.

is particularly relevant in the context of potentially habitable planet studies.

We retrieved ~40 and ~30% percentage of complex flares in both CHEOPS and TESS data, in agreement with previous studies concentrating on M stars (e.g. Davenport et al. 2014; Howard & MacGregor 2022). This suggests that stellar flares observed with future facilities will require the modelling of complex flares to correctly unveil their properties. For example, PLATO (Rauer et al. 2014) will monitor its targets at 25 s cadence. Its time resolution will reach 2.5 s for bright stars, which will also be observed in blue and red filters: therefore, we can expect it to provide large statistics about flares happening on several stellar types during its years-long continuous surveys. Ariel (Tinetti et al. 2018), instead, will be capable of 1 s cadence measurements, and might happen to resolve flare fine details during some of its exoatmosphere recognition campaigns. Both missions would benefit from further investigation in the degeneracies involved in complex flare profile fitting and false positive assessment to maximise the scientific return of their data.

Our results are qualitatively consistent with the part of Tovmassian et al. (2003)'s model that posits the peak-bump flare profile is the fundamental flare shape. Instead, we could not validate the part of their model which considers a starspot-induced, pre-flare dip as prevalent in flare profiles. Reported dip observations were made in the U, B, V, R and I bands, and spectroscopically in H_α (Leitzinger et al. 2014, and references therein): their signal would likely fall below the noise level for TESS, while they should be detectable with CHEOPS if they happened on a regular basis. However, we tentatively detected only one, $\lesssim$1 min pre-flare dip candidate, and through injection tests we found that dips are likely to be missed with CHEOPS because of the combination of data gaps and residual instrument systematics.

Our algorithm does not include the modelling of QPPs, which we visually searched in the data. Overall, ~1% of our validated flare sample could be classified as QPP candidates. We measured amplitude and period of such possible oscillations and found results in agreement with the literature, but could only identify tentative properties because of lack of statistics.

We dedicated a particular focus to the analysis of flare energy, peak luminosity, and duration distributions, and did not find significant differences in the energy and peak luminosity distributions of simple and complex flare components, contrarily to their duration distributions. As expected, we could not reach energies that might inform us on the role of micro- and nanoflares in coronal heating. Moreover, we evaluated the likelihood that an alternative description to power laws might better represent flare parameter distributions, but only found marginal preference for log-normal models with respect to power-laws in most cases, with the exception of the energy distribution of complex flare components. Verbeeck et al. (2019) found significant indications that log-normal distributions are a better fit to solar data: in this case, the unavoidable lower S/N of our data might be a limitation, and requires further investigation. In any case, our analysis supports the importance of a formal estimation of the inertial range used for the fit of power law parameters.

We also separated the flare parameter distributions occurring in partly and fully convective stars. We found significant differences in the slope of the power laws associated to earlier and later M stars peak luminosity and duration, which might indicate a selection effect as well as a transition in the generation of the magnetic field from the $\alpha\Omega$ to the α^2 dynamo process (e.g. Chabrier & Küker 2006).

The detailed exploration of power law distributions and their alternatives needs large samples to be statistically stable. Statistical frameworks such as the one by Clauset et al. (2009) and (Klaus et al. 2011) were built to maintain stability also in the case of samples with just a few hundred elements; however, we showed through simulated data sets that investigations on larger and possibly more diverse samples could shed more light on these aspects. This will surely benefit from the ultra-high precision, high-cadence, and in few cases two-coloured PLATO observations.

Acknowledgements. We thank Antonino F. Lanza and Daniel Brito de Freitas for their suggestions and the very fruitful discussions we had. This research has made use of the SIMBAD database, operated at CDS, Strasbourg, France. Our search was helped by the use of the ASTROQUERY package (Ginsburg et al. 2019). CHEOPS is an ESA mission in partnership with Switzerland with important contributions to the payload and the ground segment from Austria, Belgium, France, Germany, Hungary, Italy, Portugal, Spain, Sweden, and the United Kingdom. The CHEOPS Consortium would like to gratefully acknowledge the support received by all the agencies, offices, universities, and industries involved. Their flexibility and willingness to explore new approaches were essential to the success of this mission. CHEOPS data analysed in this article will be made available in the CHEOPS mission archive (https://cheops.unige.ch/archive_browser/). L.B., G.B., V.N., I.P., G.P., R.R., and G.S. acknowledge support from CHEOPS ASI-INAF agreement n. 2019-29-HH.0. A.B. was supported by the SNSA. P.M. acknowledges support from STFC research grant number ST/R000638/1. S.G.S. acknowledges support from FCT through FCT contract nr. CEECIND/00826/2018 and POPH/FSE (EC). The Portuguese team thanks the Portuguese Space Agency for the provision of financial support in the framework of the PRODEX Programme of the European Space Agency (ESA) under contract number 4000142255. V.V.G. is an F.R.S-FNRS Research Associate. Z.G. was supported by the VEGA grant of the Slovak Academy of Sciences No. 2/0031/22 and by the Slovak Research and Development Agency – the contract No. APVV-20-0148. G.M.S. acknowledges the support of the Hungarian National Research, Development and Innovation Office (NKFIH) grant K-125015, a PRODEX Experiment Agreement No. 4000137122, the Lendület LP2018-7/2021 grant of the Hungarian Academy of Science and the support of the city of Szombathely. D.G. gratefully acknowledges financial support from the CRT foundation under Grant No. 2018.2323 "Gaseousor rocky? Unveiling the nature of small worlds". Y.Al. acknowledges support from the Swiss National Science Foundation (SNSF) under grant 200020_192038. We acknowledge financial support from the Agencia Estatal de Investigación of the Ministerio de Ciencia e Innovación MCIN/AEI/10.13039/501100011033 and the ERDF "A way of making Europe" through projects PID2019-107061GB-C61, PID2019-107061GB-C66, PID2021-125627OB-C31, and PID2021-125627OB-C32, from the Centre of Excellence "Severo Ochoa" award to the Instituto de Astrofísica de Canarias (CEX2019-000920-S), from the Centre of Excellence "María de Maeztu" award to the Institut de Ciències de l'Espai (CEX2020-001058-M), and from the Generalitat de Catalunya/CERCA programme. We acknowledge financial support from the Agencia Estatal de Investigación of the Ministerio de Ciencia e Innovación MCIN/AEI/10.13039/501100011033 and the ERDF "A way of making Europe" through projects PID2019-107061GB-C61, PID2019-107061GB-C66, PID2021-125627OB-C31, and PID2021-125627OB-C32, from the Centre of Excellence "Severo Ochoa" award to the Instituto de Astrofísica de Canarias (CEX2019-000920-S), from the Centre of Excellence "María de Maeztu" award to the Institut de Ciències de l'Espai (CEX2020-001058-M), and from the Generalitat de Catalunya/CERCA programme. S.C.C.B. acknowledges support from FCT through FCT contracts nr. IF/01312/2014/CP1215/CT0004. C.B. acknowledges support from the Swiss Space Office through the ESA PRODEX program. This work has been carried out within the framework of the NCCR PlanetS supported by the Swiss National Science Foundation under grants 51NF40_182901 and 51NF40_205606. A.C.C. acknowledges support from STFC consolidated grant numbers ST/R000824/1 and ST/V000861/1, and UKSA grant number ST/R003203/1. P.E.C. is funded by the Austrian Science Fund (FWF) Erwin Schroedinger Fellowship, program J4595-N. This project was supported by the CNES. S.S. acknowledges support from CNES, the Programme National de Planétologie (PNP), and the Programme National de Physique Stellaire (PNPS) of CNRS-INSU. The Belgian participation to CHEOPS has been supported by the Belgian Federal Science Policy Office (BELSPO) in the framework of the PRODEX Program, and by the University of Liège through an ARC grant for Concerted Research Actions financed by the Wallonia-Brussels Federation. L.D. thanks the Belgian Federal Science Policy Office (BELSPO) for the provision of financial support in the framework of the PRODEX Programme of the European Space Agency (ESA) under contract number 4000142531. This work was supported by FCT – Fundação para a Ciência e a Tecnologia through national funds and by FEDER through COMPETE2020 through the research grants UIDB/04434/2020, UIDP/04434/2020, 2022.06962.PTDC. O.D.S.D. is supported in the form of work contract (DL 57/2016/CP1364/CT0004) funded by national funds through FCT. B.-O.D. acknowledges support from the Swiss State Secretariat for Education, Research and Innovation (SERI) under contract number MB22.00046. This project has received funding from the Swiss National Science Foundation for project 200021_200726. It has also been carried out within the framework of the National Centre of Competence in Research PlanetS supported by the Swiss National Science Foundation under grant 51NF40_205606. The authors acknowledge the financial support of the SNSF. M.F. and C.M.P. gratefully acknowledge the support of the Swedish National Space Agency (DNR 65/19, 174/18). M.G. is an F.R.S.-FNRS Senior Research Associate. M.N.G. is the ESA CHEOPS Project Scientist and Mission Representative, and as such also responsible for the Guest Observers (GO) Programme. MNG does not relay proprietary information between the GO and Guaranteed Time Observation (GTO) Programmes, and does not decide on the definition and target selection of the GTO Programme. C.He. acknowledges support from the European Union H2020-MSCA-ITN-2019 under Grant Agreement no. 860470 (CHAMELEON). S.H. gratefully acknowledges CNES funding through the grant 837319. K.G.I. is the ESA CHEOPS Project Scientist and is responsible for the ESA CHEOPS Guest Observers Programme. She does not participate in, or contribute to, the definition of the Guaranteed Time Programme of the CHEOPS mission through which observations described in this paper have been taken, nor to any aspect of target selection for the programme. K.W.F.L. was supported by Deutsche Forschungsgemeinschaft grants RA714/14-1 within the DFG Schwerpunkt SPP 1992, Exploring the Diversity of Extrasolar Planets. This work was granted access to the HPC resources of MesoPSL financed by the Region Ile de France and the project Equip@Meso (reference ANR-10-EQPX-29-01) of the programme Investissements d'Avenir supervised by the Agence Nationale pour la Recherche. M.L. acknowledges support of the Swiss National Science Foundation under grant number PCEFP2_194576. This work was also partially supported by a grant from the Simons Foundation (PI Queloz, grant number 327127). N.C.S. acknowledges funding by the European Union (ERC, FIERCE, 101052347). Views and opinions expressed are however those of the author(s) only and do not necessarily reflect those of the European Union or the European Research Council. Neither the European Union nor the granting authority can be held responsible for them. A.S. acknowledges support from the Swiss Space Office through the ESA PRODEX program. J.V. acknowledges support from the Swiss National Science Foundation (SNSF) under grant PZ00P2_208945. N.A.W. acknowledges UKSA grant ST/R004838/1. T.W. acknowledges support from the UKSA and the University of Warwick.

References

Aboudarham, J., & Henoux, J. C. 1987, A&A, 174, 270
Airapetian, V. S., Glocer, A., Gronoff, G., Hébrard, E., & Danchi, W. 2016, Nat. Geosci., 9, 452
Airapetian, V. S., Barnes, R., Cohen, O., et al. 2020, Int. J. Astrobiol., 19, 136
Akaike, H. 1974, IEEE Trans. Automat. Control, 19, 716
Alonso-Floriano, F. J., Morales, J. C., Caballero, J. A., et al. 2015, A&A, 577, A128
Alstott, J., Bullmore, E., & Plenz, D. 2014, PLoS ONE, 9, e85777
Aschwanden, M. J. 2019, ApJ, 880, 105
Aschwanden, M. J. 2022a, ApJ, 934, 33
Aschwanden, M. J. 2022b, ApJ, 934, L3
Aschwanden, M. J., Tarbell, T. D., Nightingale, R. W., et al. 2000, ApJ, 535, 1047
Astropy Collaboration (Robitaille, T. P., et al.) 2013, A&A, 558, A33
Astropy Collaboration (Price-Whelan, A. M., et al.) 2018, AJ, 156, 123
Astropy Collaboration (Price-Whelan, A. M., et al.) 2022, ApJ, 935, 167
Bailer-Jones, C. A. L., Rybizki, J., Fouesneau, M., Demleitner, M., & Andrae, R. 2021, AJ, 161, 147
Bak, P., Tang, C., & Wiesenfeld, K. 1988, Phys. Rev. A, 38, 364
Balona, L. A., & Abedigamba, O. P. 2016, MNRAS, 461, 497
Baluev, R. V. 2008, MNRAS, 385, 1279
Barth, P., Helling, C., Stüeken, E. E., et al. 2021, MNRAS, 502, 6201
Benz, A. O. 2017, Liv. Rev. Sol. Phys., 14, 2
Benz, W., Broeg, C., Fortier, A., et al. 2021, Exp. Astron., 51, 109
Boffetta, G., Carbone, V., Giuliani, P., Veltri, P., & Vulpiani, A. 1999, Phys. Rev. Lett., 83, 4662
Bogachev, S., & Erkhova, N. 2023, Sol. Terrest. Phys., 9, 3
Bogdan, T. J., Gilman, P. A., Lerche, I., & Howard, R. 1988, ApJ, 327, 451
Brasseur, C. E., Osten, R. A., & Fleming, S. W. 2019, ApJ, 883, 88
Chabrier, G., & Küker, M. 2006, A&A, 446, 1027
Chen, H., Zhan, Z., Youngblood, A., et al. 2021, Nat. Astron., 5, 298
Clauset, A., Shalizi, C. R., & Newman, M. E. J. 2009, SIAM Rev., 51, 661
Colombo, S., Petralia, A., & Micela, G. 2022, A&A, 661, A148
Cortés-Contreras, M., Béjar, V. J. S., Caballero, J. A., et al. 2017, A&A, 597, A47
Davenport, J. R. A. 2016, IAU Symp., 320, 128

Davenport, J. R. A., Hawley, S. L., Hebb, L., et al. 2014, ApJ, 797, 122
Dillon, C. J., Jess, D. B., Mathioudakis, M., et al. 2020, ApJ, 904, 109
Dobson, A. K., Donahue, R. A., Radick, R. R., & Kadlec, K. L. 1990, ASP Conf. Ser., 9, 132
Donahue, R. A. 1993, PhD thesis, New Mexico State University, USA
Donahue, R. A., & Baliunas, S. L. 1992, ApJ, 393, L63
Doyle, J. G., Butler, C. J., Bryne, P. B., & van den Oord, G. H. J. 1988, A&A, 193, 229
Feinstein, A. D., Seligman, D. Z., Günther, M. N., & Adams, F. C. 2022, ApJ, 925, L9
Fortier, A., Simon, A. E., & Broeg, C. 2024, A&A in press, https://doi.org/10.1051/0004-6361/202348576
Gaia Collaboration (Vallenari, A., et al.) 2023, A&A, 674, A1
Giampapa, M. S., Africano, J. L., Klimke, A., et al. 1982, ApJ, 252, L39
Gillon, M., Triaud, A. H. M. J., Demory, B.-O., et al. 2017, Nature, 542, 456
Ginsburg, A., Sipőcz, B. M., Brasseur, C. E., et al. 2019, AJ, 157, 98
Grayver, A., Bower, D. J., Saur, J., Dorn, C., & Morris, B. M. 2022, ApJ, 941, L7
Greco, A., Matthaeus, W. H., Servidio, S., & Dmitruk, P. 2009, Phys. Rev. E, 80, 046401
Gryciuk, M., Siarkowski, M., Sylwester, J., et al. 2017, Sol. Phys., 292, 77
Guilluy, G., Andretta, V., Borsa, F., et al. 2020, A&A, 639, A49
Günther, M. N., Zhan, Z., Seager, S., et al. 2020, AJ, 159, 60
Haisch, B., Strong, K. T., & Rodono, M. 1991, ARA&A, 29, 275
Hall, D. S. 1991, IAU Colloq., 380, 353
Hawley, S. L., Davenport, J. R. A., Kowalski, A. F., et al. 2014, ApJ, 797, 121
Hazra, G., Vidotto, A. A., & D'Angelo, C. V. 2020, MNRAS, 496, 4017
Henoux, J. C., Aboudarham, J., Brown, J. C., van den Oord, G. H. J., & van Driel-Gesztelyi, L. 1990, A&A, 233, 577
Howard, W. S., & MacGregor, M. A. 2022, ApJ, 926, 204
Hoyer, S., Guterman, P., Demangeon, O., et al. 2020, A&A, 635, A24
Hudson, H. S. 1991, Sol. Phys., 133, 357
Jackman, J. 2020, PhD thesis, University of Warwick, UK
Jackman, J. A. G., Wheatley, P. J., Acton, J. S., et al. 2020, MNRAS, 497, 809
Jackman, J. A. G., Wheatley, P. J., Acton, J. S., et al. 2021, MNRAS, 504, 3246
Jackman, J. A. G., Shkolnik, E. L., Million, C., et al. 2023, MNRAS, 519, 3564
Jenkins, J. M., Twicken, J. D., McCauliff, S., et al. 2016, SPIE Conf. Ser., 9913, 99133E
Karoff, C., Knudsen, M. F., De Cat, P., et al. 2016, Nat. Commun., 7, 11058
Klaus, A., Yu, S., & Plenz, D. 2011, PLoS ONE, 6, e19779
Kowalski, A. F., Hawley, S. L., Wisniewski, J. P., et al. 2013, ApJS, 207, 15
Kowalski, A. F., Wisniewski, J. P., Hawley, S. L., et al. 2019, ApJ, 871, 167
Kunjaya, C., Mahasena, P., Vierdayanti, K., & Herlie, S. 2011, Ap&SS, 336, 455
Lanza, A. F., Catalano, S., Cutispoto, G., Pagano, I., & Rodono, M. 1998, A&A, 332, 541
Lanza, A. F., Rodonò, M., Pagano, I., Barge, P., & Llebaria, A. 2003, A&A, 403, 1135
Lei, W. H., Li, C., Chen, F., et al. 2020, MNRAS, 494, 975
Leitzinger, M., Odert, P., Greimel, R., et al. 2014, MNRAS, 443, 898
Lendl, M., Csizmadia, S., Deline, A., et al. 2020, A&A, 643, A94
Litvinenko, Y. E. 1996, Sol. Phys., 167, 321
Locci, D., Petralia, A., Micela, G., et al. 2022, Planet. Space J., 3, 1
Louca, A. J., Miguel, Y., Tsai, S.-M., et al. 2023, MNRAS, 521, 3333
Loyd, R. O. P., France, K., Youngblood, A., et al. 2018, ApJ, 867, 71
Lu, E. T., & Hamilton, R. J. 1991, ApJ, 380, L89
Maehara, H., Shibayama, T., Notsu, S., et al. 2012, Nature, 485, 478
Maehara, H., Shibayama, T., Notsu, Y., et al. 2015, Earth Planets Space, 67, 59
Maggio, A., Locci, D., Pillitteri, I., et al. 2022, ApJ, 925, 172
Maggio, A., Pillitteri, I., Argiroffi, C., et al. 2023, ApJ, 951, 18
Mawad, R., & Moussas, X. 2022, Ap&SS, 367, 107
McIntosh, P. S., & Donnelly, R. F. 1972, Sol. Phys., 23, 444
McQuillan, A., Mazeh, T., & Aigrain, S. 2014, ApJS, 211, 24
Mendoza, G. T., Davenport, J. R. A., Agol, E., Jackman, J. A. G., & Hawley, S. L. 2022, AJ, 164, 17
Million, C., Kolotkov, D., & Fleming, S. W. 2021, in The 20.5th Cambridge Workshop on Cool Stars, Stellar Systems, and the Sun (CS20.5), 272
Morgado, B. E., Bruno, G., Gomes-Júnior, A. R., et al. 2022, A&A, 664, L15
Nakariakov, V. M., & Melnikov, V. F. 2009, Space Sci. Rev., 149, 119
Namekata, K., Sakaue, T., Watanabe, K., et al. 2017, ApJ, 851, 91
Namekata, K., Maehara, H., Notsu, Y., et al. 2019, ApJ, 871, 187
Namekata, K., Davenport, J. R. A., Morris, B. M., et al. 2020, ApJ, 891, 103
Nardiello, D., Malavolta, L., Desidera, S., et al. 2022, A&A, 664, A163
Negri, L. H., & Vestri, C. 2017, https://zenodo.org/records/887917
Neidig, D. F. 1983, Sol. Phys., 85, 285
Neidig, D. F. 1989, Sol. Phys., 121, 261
Newville, M., Stensitzki, T., Allen, D. B., & Ingargiola, A. 2014, https://zenodo.org/records/11813
Nicholls, H., Hébrard, E., Venot, O., Drummond, B., & Evans, E. 2023, MNRAS, 523, 5681
Norman, J. P., Charbonneau, P., McIntosh, S. W., & Liu, H.-L. 2001, ApJ, 557, 891
Parker, E. N. 1988, ApJ, 330, 474
Parnell, C. E., & De Moortel, I. 2012, Philos. Trans. R. Soc. A London Ser. A, 370, 3217
Peres, G., Ventura, R., Pagano, I., & Rodono, M. 1993, A&A, 278, 179
Pietras, M., Falewicz, R., Siarkowski, M., Bicz, K., & Preś, P. 2022, ApJ, 935, 143
Pont, F., Zucker, S., & Queloz, D. 2006, MNRAS, 373, 231
Pugh, C. E., Armstrong, D. J., Nakariakov, V. M., & Broomhall, A. M. 2016, MNRAS, 459, 3659
Raetz, S., Stelzer, B., Damasso, M., & Scholz, A. 2020, A&A, 637, A22
Ramsay, G., Kolotkov, D., Doyle, J. G., & Doyle, L. 2021, Sol. Phys., 296, 162
Rauer, H., Catala, C., Aerts, C., et al. 2014, Exp. Astron., 38, 249
Ricker, G. R., Winn, J. N., Vanderspek, R., et al. 2015, J. Astron. Telesc. Instrum. Syst., 1, 014003
Rimmer, P. B., Xu, J., Thompson, S. J., et al. 2018, Sci. Adv., 4, eaar3302
Rodono, M., Pucillo, M., Sedmak, G., & de Biase, G. A. 1979, A&A, 76, 242
Rodrigo, C., Solano, E., & Bayo, A. 2012, SVO Filter Profile Service Version 1.0, IVOA Working Draft 15 October 2012
Rodríguez-Barrera, M. I., Helling, C., & Wood, K. 2018, A&A, 618, A107
Sanz-Forcada, J., Ribas, I., Micela, G., et al. 2010, A&A, 511, L8
Scandariato, G., Nascimbeni, V., Lanza, A. F., et al. 2017, A&A, 606, A134
Schrijver, C. J., & Higgins, P. A. 2015, Sol. Phys., 290, 2943
Segura, A., Walkowicz, L. M., Meadows, V., Kasting, J., & Hawley, S. 2010, Astrobiology, 10, 751
Sheikh, M. A., Weaver, R. L., & Dahmen, K. A. 2016, Phys. Rev. Lett., 117, 261101
Shibayama, T., Maehara, H., Notsu, S., et al. 2013, ApJS, 209, 5
Shimizu, T., & Tsuneta, S. 1997, ApJ, 486, 1045
Sornette, D. 2009, Int. J. Terraspace Sci. Eng., 2, 1
Sornette, D., & Ouillon, G. 2012, European Physical Journal Special Topics, 205
Soubiran, C., Le Campion, J. F., Cayrel de Strobel, G., & Caillo, A. 2010, A&A, 515, A111
Spake, J. J., Sing, D. K., Evans, T. M., et al. 2018, Nature, 557, 68
Stelzer, B., Damasso, M., Scholz, A., & Matt, S. P. 2016, MNRAS, 463, 1844
Sulis, S., Lendl, M., Cegla, H. M., et al. 2023, A&A, 670, A24
Tinetti, G., Drossart, P., Eccleston, P., et al. 2018, Exp. Astron., 46, 135
Tovmassian, H. M., Zalinian, V. P., Silant'ev, N. A., Cardona, O., & Chavez, M. 2003, A&A, 399, 647
van Driel-Gesztelyi, L., Hudson, H. S., Anwar, B., & Hiei, E. 1994, Sol. Phys., 152, 145
Venot, O., Rocchetto, M., Carl, S., Roshni Hashim, A., & Decin, L. 2016, ApJ, 830, 77
Ventura, R., Peres, G., Pagano, I., & Rodono, M. 1995, A&A, 303, 509
Verbeeck, C., Kraaikamp, E., Ryan, D. F., & Podladchikova, O. 2019, ApJ, 884, 50
Vida, K., Kővári, Z., Pál, A., Oláh, K., & Kriskovics, L. 2017, ApJ, 841, 124
Vida, K., Oláh, K., Kővári, Z., et al. 2019, ApJ, 884, 160
Virtanen, P., Gommers, R., Oliphant, T. E., et al. 2020, Nat. Methods, 17, 261
Wales, D. J., & Doye, J. P. K. 1997, J. Phys. Chem. A, 101, 5111
Walkowicz, L. M., Basri, G., Batalha, N., et al. 2011, AJ, 141, 50
Watkins, N. W., Pruessner, G., Chapman, S. C., Crosby, N. B., & Jensen, H. J. 2016, Space Sci. Rev., 198, 3
Wenger, M., Ochsenbein, F., Egret, D., et al. 2000, A&AS, 143, 9
Wheatland, M. S. 2006, Sol. Phys., 236, 313
Wheatland, M. S., & Craig, I. J. D. 2006, Sol. Phys., 238, 73
Yang, H., Liu, J., Gao, Q., et al. 2017, ApJ, 849, 36
Yang, H., Liu, J., Qiao, E., et al. 2018, ApJ, 859, 87
Yang, Z., Zhang, L., Meng, G., et al. 2023, A&A, 669, A15
Zalinian, V. P., Tovmassian, H. M., & Cardona, O. 2002, Information Bull. Variab. Stars, 5256, 1
Zimovets, I. V., McLaughlin, J. A., Srivastava, A. K., et al. 2021, Space Sci. Rev., 217, 66

[1] INAF, Osservatorio Astrofisico di Catania, Via S. Sofia 78, 95123 Catania, Italy
e-mail: giovanni.bruno@inaf.it
[2] Department of Astronomy, Stockholm University, AlbaNova University Center, 10691 Stockholm, Sweden
[3] Astrophysics Group, Lennard Jones Building, Keele University, Staffordshire, ST5 5BG, UK
[4] Weltraumforschung und Planetologie, Physikalisches Institut, University of Bern, Gesellschaftsstrasse 6, 3012 Bern, Switzerland

[5] Center for Space and Habitability, University of Bern, Gesellschaftsstrasse 6, 3012 Bern, Switzerland
[6] Instituto de Astrofisica e Ciencias do Espaco, Universidade do Porto, CAUP, Rua das Estrelas, 4150-762 Porto, Portugal
[7] Aix Marseille Univ., CNRS, CNES, LAM, 38 rue Frédéric Joliot-Curie, 13388 Marseille, France
[8] Space sciences, Technologies and Astrophysics Research (STAR) Institute, Université de Liège, Allée du 6 Août 19C, 4000 Liège, Belgium
[9] HUN-REN-ELTE Exoplanet Research Group, 9700 Szombathely, Szent Imre, h. u. 112, Hungary
[10] ELTE Gothard Astrophysical Observatory, 9700 Szombathely, Szent Imre, h. u. 112, Hungary
[11] Astronomical Institute, Slovak Academy of Sciences, 05960 Tatranská Lomnica, Slovakia
[12] Konkoly Observatory, HUN-REN Research Centre for Astronomy and Earth Sciences, Konkoly Thege út 15-17., 1121 Budapest, Hungary
[13] CSFK, MTA Centre of Excellence, Konkoly Thege út 15-17., 1121 Budapest, Hungary
[14] Dipartimento di Fisica, Università degli Studi di Torino, via Pietro Giuria 1, 10125 Torino, Italy
[15] Instituto de Astrofísica de Canarias, Vía Láctea s/n, 38200 La Laguna, Tenerife, Spain
[16] Departamento de Astrofísica, Universidad de La Laguna, Astrofísico Francisco Sanchez s/n, 38206 La Laguna, Tenerife, Spain
[17] Admatis, 5. Kandó Kálmán Street, 3534 Miskolc, Hungary
[18] Depto. de Astrofísica, Centro de Astrobiología (CSIC-INTA), ESAC campus, 28692 Villanueva de la Cañada (Madrid), Spain
[19] Departamento de Fisica e Astronomia, Faculdade de Ciencias, Universidade do Porto, Rua do Campo Alegre, 4169-007 Porto, Portugal
[20] Space Research Institute, Austrian Academy of Sciences, Schmiedlstrasse 6, 8042 Graz, Austria
[21] Observatoire astronomique de l'Université de Genève, Chemin Pegasi 51, 1290 Versoix, Switzerland
[22] INAF, Osservatorio Astronomico di Padova, Vicolo dell'Osservatorio 5, 35122 Padova, Italy
[23] Centre for Exoplanet Science, SUPA School of Physics and Astronomy, University of St Andrews, North Haugh, St Andrews KY16 9SS, UK
[24] Institute of Planetary Research, German Aerospace Center (DLR), Rutherfordstrasse 2, 12489 Berlin, Germany
[25] INAF, Osservatorio Astrofisico di Torino, Via Osservatorio, 20, 10025 Pino Torinese To, Italy
[26] Centre for Mathematical Sciences, Lund University, Box 118, 221 00 Lund, Sweden
[27] Astrobiology Research Unit, Université de Liège, Allée du 6 Août 19C, 4000 Liège, Belgium
[28] Institute of Astronomy, KU Leuven, Celestijnenlaan 200D, 3001 Leuven, Belgium
[29] Centre Vie dans l'Univers, Faculté des sciences, Université de Genève, Quai Ernest-Ansermet 30, 1211 Genève 4, Switzerland
[30] Leiden Observatory, University of Leiden, PO Box 9513, 2300 RA Leiden, The Netherlands
[31] Department of Space, Earth and Environment, Chalmers University of Technology, Onsala Space Observatory, 439 92 Onsala, Sweden
[32] Department of Astrophysics, University of Vienna, Türkenschanzstrasse 17, 1180 Vienna, Austria
[33] European Space Agency (ESA), European Space Research and Technology Centre (ESTEC), Keplerlaan 1, 2201 AZ Noordwijk, The Netherlands
[34] Institute for Theoretical Physics and Computational Physics, Graz University of Technology, Petersgasse 16, 8010 Graz, Austria
[35] Konkoly Observatory, Research Centre for Astronomy and Earth Sciences, 1121 Budapest, Konkoly Thege Miklós út 15-17, Hungary
[36] ELTE Institute of Physics, Pázmány Péter sétány 1/A, 1117 Budapest, Hungary
[37] IMCCE, UMR8028 CNRS, Observatoire de Paris, PSL Univ., Sorbonne Univ., 77 av. Denfert-Rochereau, 75014 Paris, France
[38] Institut d'astrophysique de Paris, UMR7095 CNRS, Université Pierre & Marie Curie, 98bis bd. Arago, 75014 Paris, France
[39] Institute of Optical Sensor Systems, German Aerospace Center (DLR), Rutherfordstrasse 2, 12489 Berlin, Germany
[40] Dipartimento di Fisica e Astronomia "Galileo Galilei", Università degli Studi di Padova, Vicolo dell'Osservatorio 3, 35122 Padova, Italy
[41] Department of Physics, University of Warwick, Gibbet Hill Road, Coventry CV4 7AL, UK
[42] ETH Zurich, Department of Physics, Wolfgang-Pauli-Strasse 2, 8093 Zurich, Switzerland
[43] Cavendish Laboratory, JJ Thomson Avenue, Cambridge CB3 0HE, UK
[44] Institut fuer Geologische Wissenschaften, Freie Universitaet Berlin, Maltheserstrasse 74-100,12249 Berlin, Germany
[45] Institut de Ciencies de l'Espai (ICE, CSIC), Campus UAB, Can Magrans s/n, 08193 Bellaterra, Spain
[46] Institut d'Estudis Espacials de Catalunya (IEEC), Gran Capità 2-4, 08034 Barcelona, Spain
[47] Institute of Astronomy, University of Cambridge, Madingley Road, Cambridge, CB3 0HA, UK

Appendix A: Target list and TESS proposal reference

Table A.1: List of targets and related parameters.

Name	GAIA G mag	$T_{\rm eff}$ [K]	$v \sin i$ [km s^{-1}]	$\log R'_{\rm HK}$	Distance [pc]
2MASS J00503319+2449009	11.22	3122.25	10.4		14.98
2MASS J03121265+2951325	10.47	4201.63	18.3		36.55
2MASS J03413724+5513068	10.55	4050.0	4.5		35.77
2MASS J05280015+0938382	11.18	3425.0	2.6		10.21
2MASS J06144242+4727346	10.81	3739.48	7.3		37.3
2MASS J06192947+1357031	10.01	3739.48	1.0		25.01
2MASS J08115757+0846220	11.38	3122.25	2.5		6.77
2MASS J09304457+0019214	10.49	3275.05	1.6		9.91
2MASS J11285624+1010395	11.34	3122.25	1.7		12.77
2MASS J11421839+2301365	10.83	3739.48	1.0		30.86
2MASS J11474440+0048164	9.59	3122.25	3.7	-5.5	3.37
2MASS J13314666+2916368	10.61	3122.25	55.8	-4.0	
2MASS J14511044+3106406	11.3	3122.25	2.2		13.04
2MASS J18361922+1336261	11.15	3122.25	1.6	-4.76	12.02
2MASS J20103444+0632140	10.92	3122.25	1.0		16.08
2MASS J21462206+3813047	10.82	2971.27	1.4		7.04
2MASS J22232904+3227334	10.35	3350.0	8.5	-4.1	15.22
2MASS J22561349+5919087	10.65	3739.48	1.0		46.21
2MASS J23415498+4410407	10.37	2971.27	2.5		3.16
2MASS J23430628+3632132	11.15	3122.25	2.2		8.36
AD Leo	8.21	4363.0	3.5		4.96
AU Mic	7.84	3642.0	8.5	-4.11	9.71
BD+33 1505	9.35	3619.0	3.7		18.21
BD-02 2198	9.12	3866.0	3.2		14.23
BX Cet	10.32	3275.05	3.0		7.22
CE Boo	9.13	3780.0	4.3		9.94
EE Leo	10.28	3122.25	2.6		6.96
EQ Peg	9.04	3630	16.0		6.26
EG Cam	9.41	3739.48	2.3		13.48
EV Lac	9.0	3122.25	5.1		5.05
G 168-31	10.98	3429.2	1.1		37.19
G 214-14	10.38	3739.48	1.7		23.68
G 234-57	10.46	3429.2	2.0		23.61
G 234-57	10.46	3429.2	2.0		24.31
G 32-5	11.4	3122.25	5.5		12.16
G 99-49	9.9	3275.05	5.7		5.21
GJ 1	7.68	3429.2	2.8		4.35
GJ 1074	10.15	3584.18	4.0		21.04
GJ 1105	10.67	3275.05	1.9		8.85
GJ 15 A	7.22	3605.5	3.7		3.56
GJ 160.2	9.2	4498.0	1.0		25.86
GJ 162	9.36	4201.63	2.4		13.92
GJ 176	9.0	3679.0	12.6		9.48
GJ 180	9.93	3275.05	1.7		11.94
GJ 184	9.21	3739.48	3.5		13.85
GJ 2	9.08	3875.0	1.8		11.5
GJ 205	7.1	3731.2	3.3		5.7
GJ 2066	9.12	3429.2	1.9		8.94
GJ 229	7.31	3814.0	3.1		5.76
GJ 26	10.05	3429.2	2.2		12.67
GJ 273	8.59	3275.05	2.2		3.79
GJ 3138	10.19	3894.54	1.0		28.45
GJ 317	10.75	3275.05	2.8		15.17
GJ 328	9.29	3739.48	3.4		20.5
GJ 3304	12.12	3122.25	24.0		13.1
GJ 3323	10.65	3122.25	2.3		5.37
GJ 358	9.63	3275.05	1.6		9.6

Table A.1: continued.

Name	GAIA G mag	$T_{\rm eff}$ [K]	$v \sin i$ [km s^{-1}]	$\log R'_{\rm HK}$	Distance [pc]
GJ 3649	9.88	3584.18	1.9		16.68
GJ 382	8.33	3429.2	2.2		7.7
GJ 3822	9.83	3584.18	3.5		20.34
GJ 399	10.26	3429.2	1.7		15.57
GJ 3997	9.64	3739.48	2.7		13.68
GJ 408	8.97	3122.25	2.1		6.75
GJ 4092	10.12	3739.48	2.7	-4.79	28.27
GJ 422	10.48	3275.05	1.2	-5.83	12.67
GJ 433	8.89	3616.0	1.3	-5.22	9.07
GJ 436	9.57	3416.0	1.7		9.77
GJ 450	8.85	3584.18	5.8		8.76
GJ 47	9.84	4104.0	2.0		10.53
GJ 49	8.66	4055.5	2.9		9.86
GJ 494	8.91	3899.5	9.1	-4.0	11.5
GJ 514	8.21	3727.0	1.9	-5.1	7.63
GJ 521	9.4	3584.18	2.9		13.36
GJ 526	7.61	3634.0	2.4	-5.27	5.43
GJ 536	8.86	4067.0	1.7		10.42
GJ 552	9.72	3429.2	2.6	-5.13	14.21
GJ 581	9.41	3442.0	1.8	-5.77	6.3
GJ 588	8.27	3429.2	1.8	-5.38	5.92
GJ 606	9.59	3584.18	2.0	-4.78	13.27
GJ 609	11.16	3122.25	2.0	-5.76	10.02
GJ 628	8.79	3570.0	1.5	-5.52	4.31
GJ 649	8.82	3696.33	2.1	-5.0	10.39
GJ 65	10.81	2971.27	26.4		2.72
GJ 667 C	9.39	4880.0	1.4		7.24
GJ 674	8.33	3275.05	1.8	-5.08	4.55
GJ 676 A	8.87	3739.48	2.6	-4.76	15.97
GJ 686	8.74	3584.18	2.9	-5.18	8.16
GJ 699	8.2	3244.67	2.5	-5.56	1.83
GJ 70	9.9	3429.2	2.0		11.32
GJ 701	8.52	3630.0	1.9	-5.09	7.74
GJ 731	9.38	3739.48	2.7		15.2
GJ 740	8.46	3584.18	2.3	-4.63	11.1
GJ 752 A	8.1	3275.05	2.7	-5.28	5.91
GJ 83.1	10.67	3122.25	2.6	-4.79	4.47
GJ 832	7.74	3707.0	2.0	-5.07	4.97
GJ 846	8.4	3580.0	3.1		10.57
GJ 849	9.22	3275.05	1.7	-5.4	8.81
GJ 876	8.88	3532.0	2.5	-5.7	4.67
GJ 880	7.79	3750.0	2.4		6.87
GJ 908	8.15	3646.0	2.6		5.91
GJ 9122 B	9.92	3739.48	3.6		17.22
GJ 9404	9.87	3739.48	2.6		23.84
GJ 9440	9.71	3429.2	2.6	-5.11	16.85
GJ 9793	10.04	3739.48	1.0		30.91
Gl 799B	9.6	3123.0	10.2		9.8
Gl 841 A	9.41	3429.2	4.2		14.86
HD 154363B	9.17	3584.18	2.7	-5.57	10.46
HD 233153	8.91	5125.96	2.7		12.27
HD 265866	8.86	3275.05	1.7		5.58
HD 50281B	9.09	4763.86	3.9		8.75
HD 95735	6.6	3563.5	7.3		2.55
HD 98712A	8.75	4875.0	4.2		13.72
HIP 12961	9.6	4131.0	1.2		23.41
HIP 57050	10.58	3122.25	1.8		11.02
HIP 79431	10.24	3275.05	1.0		14.56
LHS 3432	9.8	3429.2	4.3	-4.93	8.83
LP 609-71	9.61	3429.2	2.7		
LP 672-42	10.81	3275.05	1.5		13.47

Table A.1: continued.

Name	GAIA G mag	$T_{\rm eff}$ [K]	$v \sin i$ [km s^{-1}]	$\log R'_{\rm HK}$	Distance [pc]
LP 687-17	11.38	3122.25	2.4		19.57
MCC 549	10.28	3739.48	19.1		38.79
Proxima Centauri	8.95	2990.5	2.6		1.3
Ross 45A	11.29	3275.05	3.7		22.12
Ross 733	10.37	3122.25	14.0		18.11
TYC 1313-1482-1	10.27	3739.48	1.0		
TYC 4902-210-1	10.01	3739.48	1.6		31.11
V1054 Oph	8.27	3200	2.1		
V1352 Ori	10.1	3122.25	4.7		5.79
VV Lyn	9.59	3429.2	4.6		11.99
Wolf 906	10.17	3429.2	1.7		14.48
YZ Ceti	10.43	3122.25	2.2		3.72

Table A.2: PIs and TESS programmes for which 20 s light curves of our targets were obtained.

PI	Programmes
Aloisi, Robert	G05115
Barnes, Sydney	G03182
Burt, Jennifer	G03272, G04191
Cloutier, Ryan	G03274, G04214. G05152
Davenport, James	G03227, G04039
Gillen, Edward	G05106
Guenther, Maximilian	G05143
Hambleton, Kelly	G03252
Hermes, James	G04137, G03124, G05081
Holberg, Jay	G03178
Hord, Benjamin	G05015
Howard, Ward	G03174, G04132, G05064
Huber, Daniel	G04103, G03251, G05144
Inglis, Andrew	G04186
Jackman, James	G04142, G04139, G05112, G05114, G05126
Kaltenegger, Lisa	G04147
Kane, Stephen	G03106, G04098
Kiman, Rocio	G05123
Kunimoto, Michelle	G04036
Llama, Joe	G03063
Lopez, Eric	G03126
Macgregor, Meredith	G05070
Marocco, Federico	G04211, G05109
Martin, David	G05071
Mayo, Andrew	G03278, G04242
Million, Chase	G03228
Monsue, Teresa	G04222, G03205
Newton, Elisabeth	G03141
Paudel, Rishi	G04212, G03202
Pepper, Joshua	G04178
Pietras, Malgorzata	G05145
Pineda, J. Sebastian	G03225
Plavchan, Peter	G03263
Prsa, Andrej	G05003
Ramsay, Gavin	G04006
Robertson, Paul	G04059, G04148
Silverstein, Michele	G03226, G04188
Taylor, Jake	G03276
Tovar Mendoza, Guadalupe	G05121
Vanderburg, Andrew	G04200, G03207, G05084
Vega, Laura	G03273
Winters, Jennifer	G04033, G03250, G05087

Appendix B: Quasi-periodic pulsation additional candidates

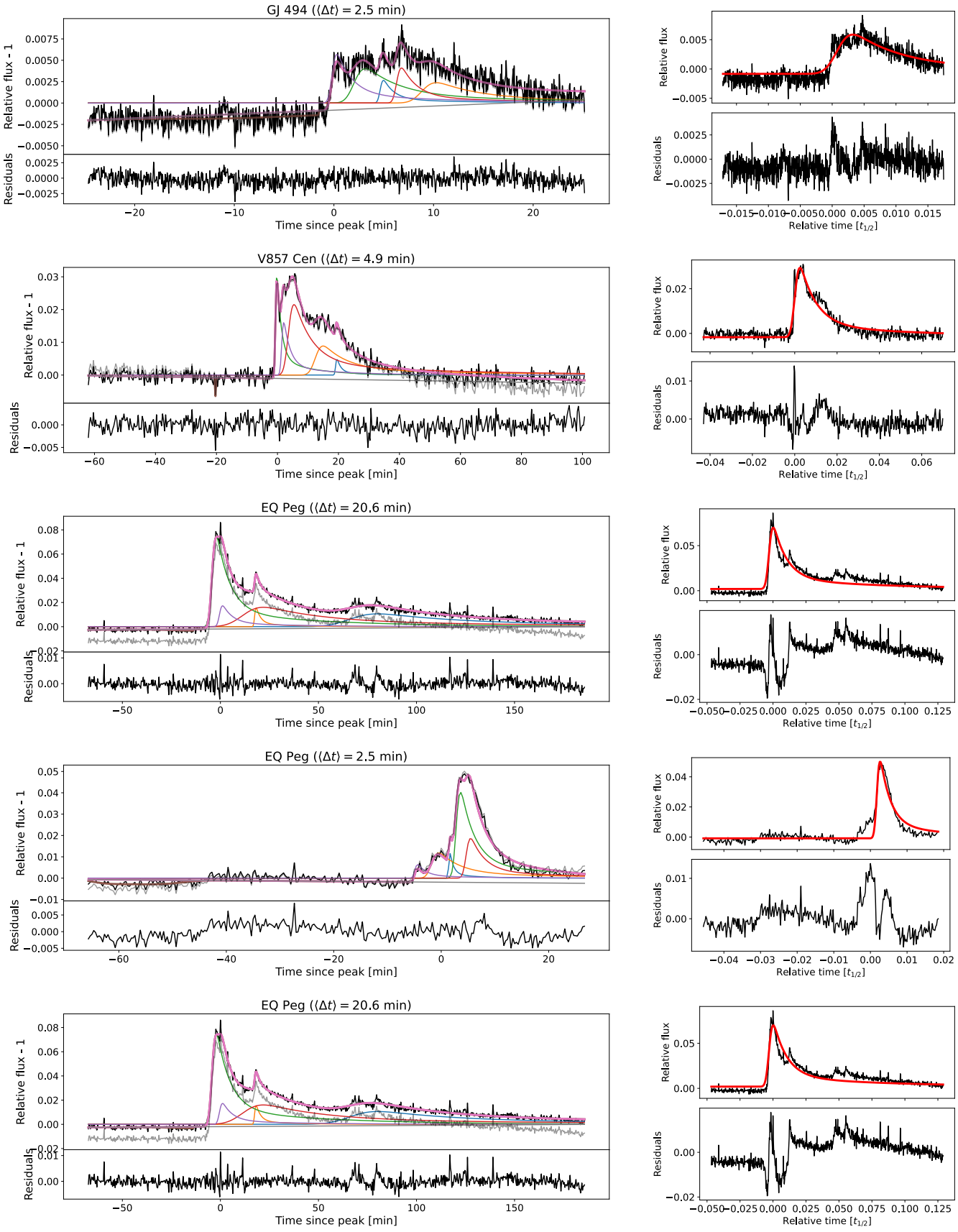

Fig. B.1: QPP candidates not shown in the main text. Each row represents a different candidate, and its description is the same as in Figure 19 (first part).

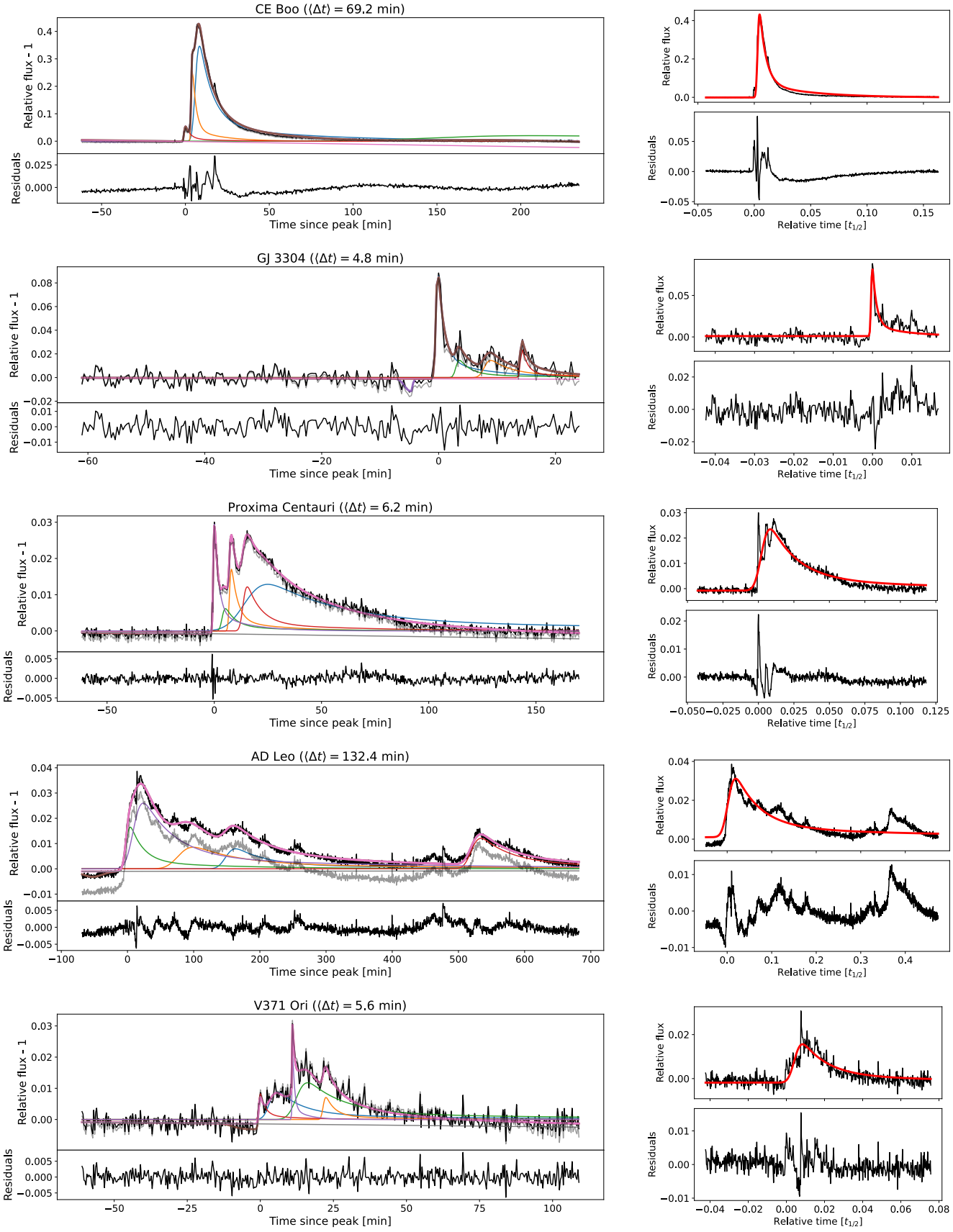

Fig. B.1: continued. The fourth candidate in this Figure (observed on AD Leo) was not used for the calculation of the median flare residual periodicity (Section 6.7), because of its associated poor fit.

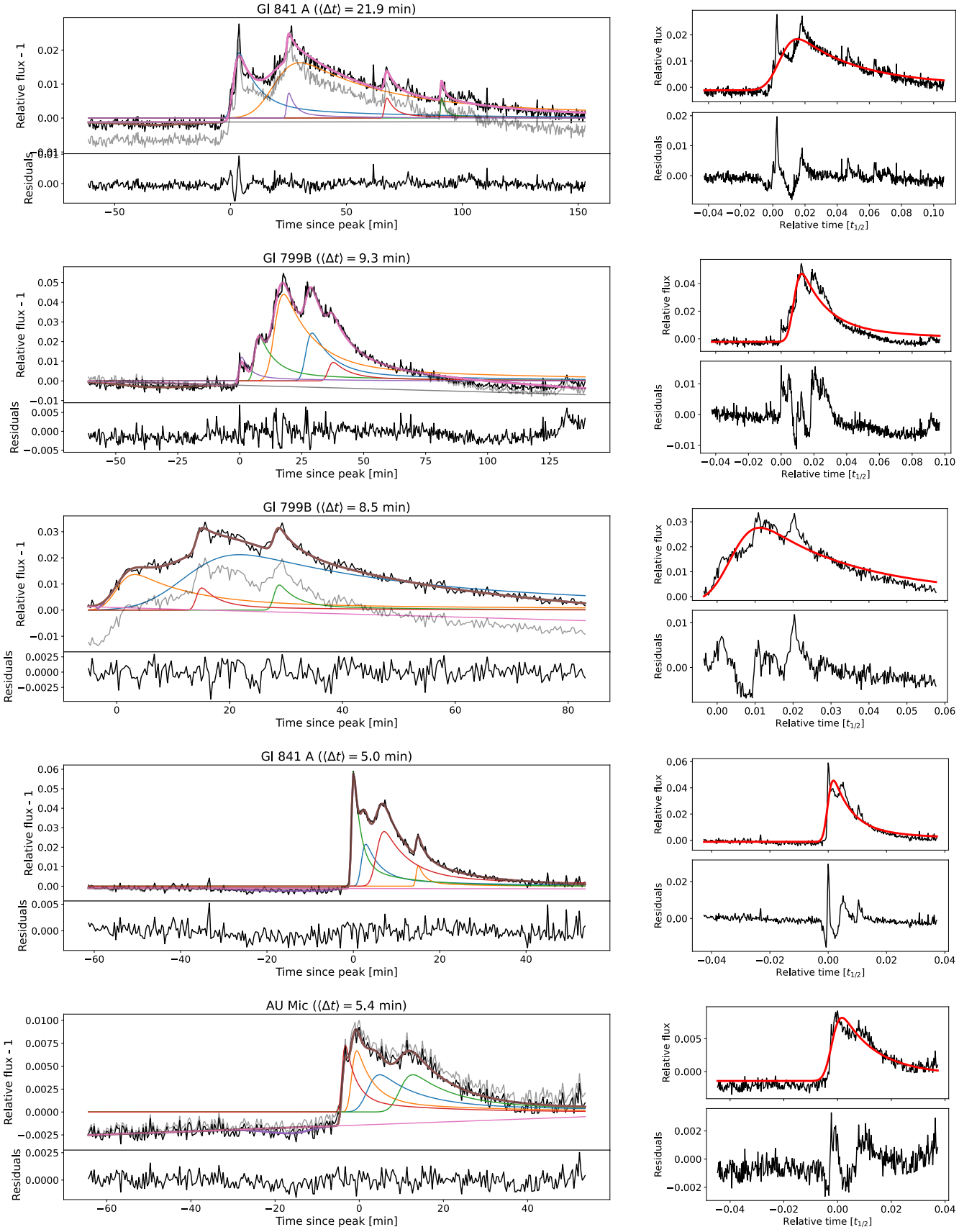

Fig. B.1: continued.